Transactions of the TSME (2019) Vol. 7, No. 2, 122-133
Journal of Research and Applications in Mechanical Engineering

ISSN 2229-2152 print
DOI: 10.14456/jrame.2019.12

Research Article

NUMERICAL ANALYSES OF MICRO HYGRO-MECHANICAL BEHAVIOURS OF WOOD FIBRE REINFORCED COMPOSITES

N. Charupeng*
K. Prapot
Department of Mechanical Engineering, Faculty of Engineering, Kasetsart University, 50 Ngam Wong Wan Rd., Lat Yao, Chatuchak, Bangkok 10900, Thailamd

Received 25 April 2019
Revised 27 May 2019
Accepted 27 May 2019

ABSTRACT:
In spite of their relatively low manufacturing costs and enhanced mechanical properties, wood fibre-reinforced composite materials have a number of drawbacks regarding the long-term durability. One of which, as commonly known, arises from the hygroexpansion subjected to moisture uptake. Various experimental studies have been performed to investigate the mechanical behaviours in multi-scale while considerably less attempts on micromechanical studies are published. This research is presented to simulate the hygroelastic behaviours of wood fibre-reinforced composites in microscopic scale. Hygroelastic strains in orthotropic directions are accounted for. Weak formulation Finite Element Method for hygroexpansion of wood fibre constituent is developed and the algorithm is implemented using MATLAB. Input data in the model are model dimensions, elastic constants, densities of both constituents, fibre weight fraction, hygroexpansion coefficients of wood fibre and relative humidity. The simulation results exhibits reasonable agreements with the experiments - sorption tests of birch fibres-PLA matrix composite from previous studies, especially at low wood contents. The models also confirms structural failure caused by hygroexpansion. This model aims to be a preliminary design tool for creating wood fibre-reinforced composites exposed to high relative humidity. Further studies can be done to investigate debonding and cracking behaviours under wet-dry cycles.

***Keywords**: Wood fibres, Hygroelastic, Micromechanical model, Hygroexpansion, Finite Element Method*

1. INTRODUCTION

Wood fibre-reinforced composite materials, have been in construction materials industry for a few decades. The primary industrial reasons are that wood fibres or natural fibres are low-cost, lightweight, biodegradable as well as renewable. Having said that, moisture induced expansion namely hygroexpansion is one of the major drawbacks of wood-based composites. Wood-related constituents are hydrophilic, owing to the formation of numerous hydrogen bonds with the hydroxyl groups in lignin, hemicellulose and cellulose [1]. Such formation leads to hygroelastic swelling of wood fibres. Unlike wood fibres, matrix constituents in wood-based composites such as polymer and cement are hydrophobic, that is, they are much less susceptible to water and moisture uptake compared to wood.

The drastic difference in hygroelastic properties have been found to compromise the durability of the composites. Most of literature findings postulated that moisture movement is the main cause of reduced durability in wood-cement

* Corresponding author: N. Charupeng
E-mail address: nuttibase.c@live.ku.th

composites (WCCs) [2], such as, a decresse in post-cracking strength. An extensive review for cellulose fibre-cement composite naturally aged over 5 years by Cooke [3] has suggested that moisture cycling is part of the most effective weathering that deteriorates the long-term mechanical properties, especially toughness of the composites. Mohr et. al. [4] performed an experimental study with kraft pulp fibre-cement composites and proposed a degradation mechanism under wet-dry cycling, which progresses from fibre-cement debonding, mineralization and ultimately fibre embrittlement.

In wood-polymer composites (WPCs), the swelling effects due to moisture even result in physically obvious problems, such as buckling and distortion of installed WPC boards [5]. Like WCCs, WPCs suffer from moisture-induced degradation mechanism. Swelling and shrinking initiates the breaking of interfacial bonds between the constituents, which in turns, creates either microcracks in plastic and leaving no adhesion at the interfaces or internal fracture of wood particles due to re-strained swelling [6]. Furthermore, moisture content usually results in a decrease in the elastic modulus of wood fibres [7]. Another study [8] also showed that, when water soaked, a WPC with moderate wood content could have significantly reduced flexural properties. Recently, there has been an extensive overview by Lindner [9], concluding that the dominant factors affecting hygroexpansion of wood are single fibre sorption, interfacial contacts, microfibril angle, fibre morphology as well as fibre orientation.

From above, one must acknowledge the importance of lowering the moisture effects on structural integrity of wood fibres composites. As aforementioned, the deterioration of mechanical properties of wood fibres composites resulted from moisture cycling occurs in a progressive manner for an extended time period [3, 4]. Therefore, the accurate method of predicting the durability would be to microscopically investigate the hygro-mechanical behaviours of wood fibres and matrix constituents, subjected to progressive wet-dry cycling. This requires a robust quantitative analysis that enables local stresses at the interfaces to be analysed. It can also be used for further studies on crack initiation and propagation for life prediction of the composites.

Since late 1990s, Finite Element (FE) numerical simulation techniques have been continuously improved and made possible for modelling and analyzing a composite structure with multiple fibres [10, 11] as well as randomly oriented fibre network [12, 13]. Xiong, X et. al. [14] have recently conducted a comprehensive review of FE-based models of natural fibres reinforced composites, studying only the micromechanical and thermal properties but not hygro-mechanical properties.

Stålne, K & Gustafsson, P-J [15] presented a validated analytical 3-D model to calculate the stiffness and hygroexpansion of fibre and particle composite materials, relying on homogenized polymer-coated single fibre modelling. Another study with similar concepts [16] came up with a micromechanical analytical model to predict the crack initiation in WPCs under moist environments. Meanwhile, Kristofer et. al. [17] performed a numerical study based on 2-D plane-strain micromechanical simulation on the swelling in the radial direction of single wood fibre surrounded by PLA matrix. It was suggested that the discrepancy of predicted and experimental results were owing to the hygroexpansion from resin filled lumens not being accounted for. Therefore, the lack of extensive studies in modelling of hygroelasticity in wood composites with randomly dispersed short fibres has given rise to the current work.

In the present work, the objective is to present a micromechanical model of wood-fibre polymer matrix composite, with irregular orientation of multiple dispersed fibres. The model is FE-based and 2-D, using quadrilateral bilinear element square elements with a uniform element size. As the model is not intended to provide calculated laminate properties, homogenization is not in use. Simulation results of hygroelastic strain in the vertical y-direction are of interest. The model is validated with results from a previous study [18]. Von Mises stresses at interfaces are also calculated and discussed. This model aims to be a preliminary design tool for creating wood fibre-reinforced composites exposed to high relative humidity.

2. MODELLING THEORY AND METHODOLOGY

Geometry pre-processing, solving as well as data post-processing are done via MATLAB©2018a. The model is fundamentally based on Finite Element Formulation, where reasonable simplification and assumptions are made.

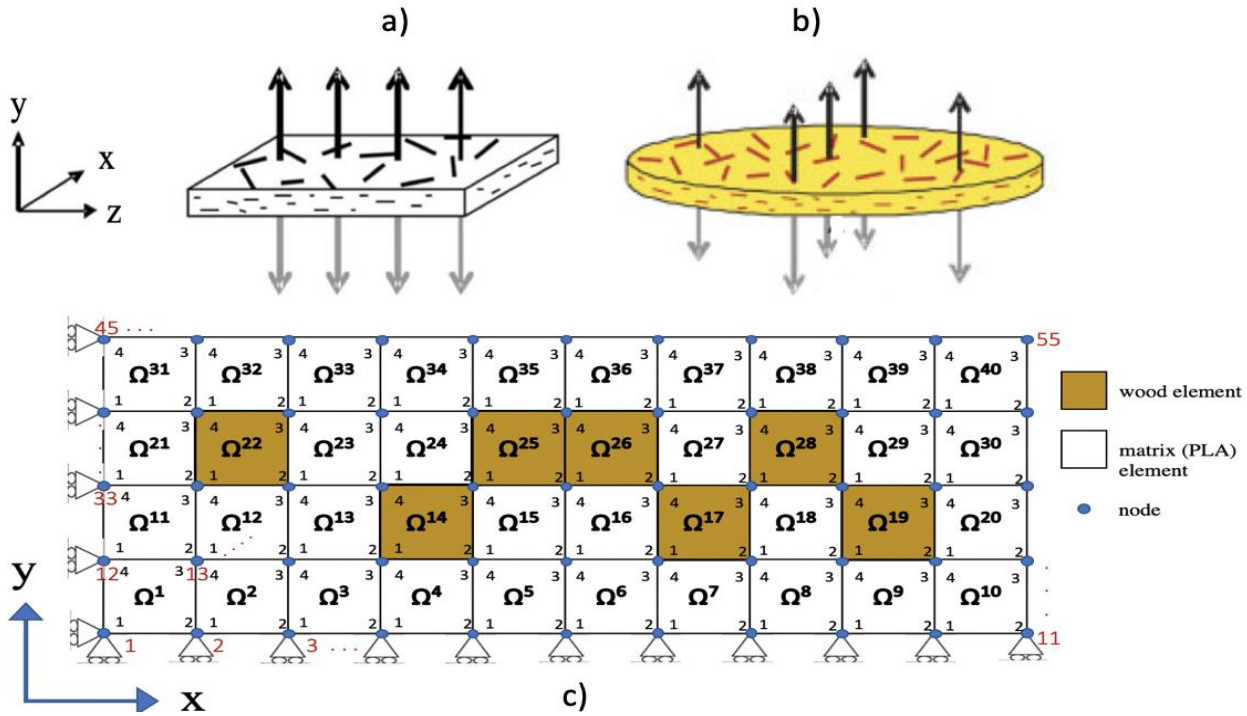

Fig. 1. a) Out-of-plane (y-direction) hygroexpansion of study [18]; sample dimensions(x,y): 20mm x 1.5mm. b) Out-of-plane(y-direction) hygroexpansion of study [19];sample dimensions(x,y):50mm x 4mm; where axes are modified for ease of comparison and consistency. c) Example of 55-node FE model of 10x4 elements; wood (brown), PLA (white) elements and nodes are numbered as shown. 1-4 local nodes in anti-clockwise direction. Global nodes in red; global coordinates generated from bottom left: node1 (0,0) to top right: node55 (10,4). Rollers indicate constraints in the supported directions.

2.1 FE model and model simplification

For reliability of validation, two studies [18, 19] on the same composite system, i.e. birch fibres being the fibre and PLA being the matrix constituents, are compared to our numerical results. Fig.1a)-b) show the actual (not to scale) specimens. In [18] (see Fig.1a), the actual specimen is a rectangular plate whose dimensions on the x-y plane are 20 mm x 1.5 mm. For study [19], flat circular test specimens with a diameter of 50mm and thickness of ~4 mm were tested instead. Specimens from both studies were produced by exactly the same method except only that the composite plates are machined to produce different shapes and dimensions. Plus, all other materials parameters and selections are the same.

In our model, wood fibres are aligned such that the local coordinates T,R,L coincide with the global coordinates x,y,z respectively (see Fig.1 for comparison). Wood fibres appear as cross-sections in the x-y plane, in which each one is assumed to have a rectangular shape, which is equivalent to a single unit square element. Each element has a length of the estimated width of the fibres, which is taken from the average [20] as 30um. This leads to the numbers of elements of 666x50 on the x and y directions to compare with study [18], and of 1666x133 elements for study [19]. This helps ensure uniformity of the entire mesh.

An example 2-D FE model model of 10 by 4 elements with 55 nodes are shown in Fig.1c)

Other assumptions are described as follows: no interior space within the wood fibre, 2-D plane-strain, with $\varepsilon_{zz} = \gamma_{xz} = \gamma_{yz} = 0$, space is either occupied by wood fibre or matrix (PLA) - which means neither porosity nor void with in the fibre is considered**,** wood fibres are randomly dispersed throughout the cross-section. Interfacial bonds between wood fibres and PLA are perfect. Synthesised sheets have an even, in-plane fibre distribution and oriented fibres, meaning that there are no fibres with arrangement aligning out-of-plane to the y-direction. PLA matrix has negligible hygroexpansion upon moisture, and is isotropic, whereas wood, in this study, is assumed to be transversely isotropic.

Input data include horizontal and vertical dimensions, materials properties, relative humidity (RH), weight fraction of wood fibres (%Wtf), densities of wood fibres and matrix constituents, ρ_f and ρ_m respectively, which are all mentioned later. The elements on the four edges are not occupied by wood elements because the actual specimens in the previous study were machined to obtain smooth surfaces. Stiffness properties of both constituents are unaffected by moisture. Moisture change is always below saturation point of wood**.** Wood fibres are transversely isotropic. And the hygroexpansion of the matrix constituent is neglected compared to that of wood fibres.

2.2 Finite Element Formulation

Displacement approximation over each bilinear quadrilateral element Ω^e of weak formulation in terms of interpolation functions, i.e. $\{u^e\} = [N^e]\{d^e\}$ in the matrix form is

$$\begin{Bmatrix} u^e \\ v^e \end{Bmatrix} = \begin{bmatrix} N_1^e & 0 & N_2^e & 0 & N_3^e & 0 & N_4^e & 0 \\ 0 & N_1^e & 0 & N_2^e & 0 & N_3^e & 0 & N_4^e \end{bmatrix} \begin{Bmatrix} u_1^e \\ v_1^e \\ u_2^e \\ v_2^e \\ u_3^e \\ v_3^e \\ u_4^e \\ v_4^e \end{Bmatrix} \tag{1}$$

,where {} as a vector and [] as matrix array hereafter, [N] as interpolation functions and {d} as nodal displacements. The bilinear interpolation functions for natural system (Fig.2) are:

$$N_i(\xi,\eta) = \frac{1}{4}(1+\xi_i\xi)(1+\eta_i\eta)\ ;\ \xi_i,\eta_i \in \{-1,1\} \tag{2}$$

,where $N_1(-1,-1)\ for\ i=1\ , N_2(1,-1)\ for\ i=2, N_3(1,1)\ for\ i=3, N_4(-1,1)\ for\ i=4.\ \Delta\xi = \Delta\eta = 2; \xi = \eta = 0$ at centre of the natural element.

Strains approximation in terms of strain-displacement matrix is given as

$$\begin{Bmatrix} \varepsilon_x^e \\ \varepsilon_y^e \\ \gamma_{xy}^e \end{Bmatrix} = \begin{Bmatrix} \frac{\partial u^e}{\partial x} \\ \frac{\partial v^e}{\partial y} \\ \frac{\partial u^e}{\partial y} + \frac{\partial v^e}{\partial x} \end{Bmatrix} = [B^e]\{d^e\} =$$

$$\begin{bmatrix} \frac{\partial N_1^e(x,y)}{\partial x} & 0 & \frac{\partial N_2^e(x,y)}{\partial x} & 0 & \frac{\partial N_3^e(x,y)}{\partial x} & 0 & \frac{\partial N_4^e(x,y)}{\partial x} & 0 \\ 0 & \frac{\partial N_1^e(x,y)}{\partial y} & 0 & \frac{\partial N_2^e(x,y)}{\partial y} & 0 & \frac{\partial N_3^e(x,y)}{\partial y} & 0 & \frac{\partial N_4^e(x,y)}{\partial y} \\ \frac{\partial N_1^e(x,y)}{\partial y} & \frac{\partial N_1^e(x,y)}{\partial x} & \frac{\partial N_2^e(x,y)}{\partial y} & \frac{\partial N_2^e(x,y)}{\partial x} & \frac{\partial N_3^e(x,y)}{\partial y} & \frac{\partial N_3^e(x,y)}{\partial x} & \frac{\partial N_4^e(x,y)}{\partial y} & \frac{\partial N_4^e(x,y)}{\partial x} \end{bmatrix} \{d^e\} \tag{3}$$

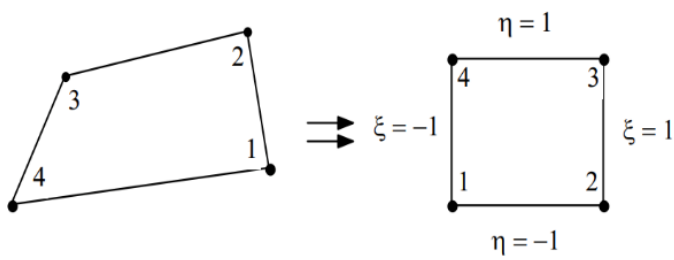

Fig. 2. Element transformation from global to natural coordinate system.

The global (x,y) coordinate system needs be transformed into natural (ξ, η) system. So, elements of B^e will be derived

$$\begin{Bmatrix} \frac{\partial N}{\partial \xi} \\ \frac{\partial N}{\partial \eta} \end{Bmatrix} = \begin{bmatrix} \frac{\partial x}{\partial \xi} & \frac{\partial y}{\partial \xi} \\ \frac{\partial x}{\partial \eta} & \frac{\partial y}{\partial \eta} \end{bmatrix} \begin{Bmatrix} \frac{\partial N}{\partial x} \\ \frac{\partial N}{\partial y} \end{Bmatrix} = [\,J\,] \begin{Bmatrix} \frac{\partial N}{\partial x} \\ \frac{\partial N}{\partial y} \end{Bmatrix} \tag{4}$$

,where [J] is non-singular Jacobian transformation matrix, and can be determined by

$$[\,J^e\,] = \begin{bmatrix} \sum_{i=1}^{m} x_i \frac{\partial \widehat{N_i}}{\partial \xi} & \sum_{i=1}^{m} y_i \frac{\partial \widehat{N_i}}{\partial \xi} \\ \sum_{i=1}^{m} x_i \frac{\partial \widehat{N_i}}{\partial \eta} & \sum_{i=1}^{m} y_i \frac{\partial \widehat{N_i}}{\partial \eta} \end{bmatrix} \tag{5}$$

,where the global coordinates of (x_i, y_i) local nodes are from node i to m over Ω^e, and interpolation functions are $\widehat{N}^e{}_i$ for geometry, which are different to N_i^e with used in the approximation.

As to transform B^e from eqn.(3) to natural system, re-arranging eqn.4 yields:

$$\begin{Bmatrix} \frac{\partial N^e(x,y)}{\partial x} \\ \frac{\partial N^e(x,y)}{\partial y} \end{Bmatrix} = [\,J\,]^{-1} \begin{Bmatrix} \frac{\partial N^e(\xi,\eta)}{\partial \xi} \\ \frac{\partial N^e(\xi,\eta)}{\partial \eta} \end{Bmatrix} = \begin{bmatrix} J_{11}^* & J_{12}^* \\ J_{21}^* & J_{22}^* \end{bmatrix} \begin{Bmatrix} \frac{\partial N^e(\xi,\eta)}{\partial \xi} \\ \frac{\partial N^e(\xi,\eta)}{\partial \eta} \end{Bmatrix} \tag{6}$$

,where J_{ij}^* is the element in position (i, j) of [J]$^{-1}$. The element area $dA \equiv dxdy$ over Ω^e is, therefore, transformed to $J\, d\xi d\eta$. Therefore, integration over element in global system becomes

$$\int_{\Omega^e}(\,)\, dxdy = \int_{-1}^{1}\int_{-1}^{1}(\,)\,|\,\mathrm{J}\,|\, d\xi d\eta \tag{7}$$

Substituting displacements and weight functions being into the weak formulations of second-order differential governing equations of plane elasticity, followed by integrating yields

$$[K^e]\{d^e\} = \{f^e\} + \{Q^e\} \tag{8}$$

From eqn.(7), $[K^e]$ is transformed into natural system as

$$[K^e] = t\int_{\Omega^e}[B^e]^T[D^e][B^e]dxdy = t\int_{-1}^{1}\int_{-1}^{1}\ [B^e]^T[D^e][B^e]|\,\mathrm{J}\,|d\xi d\eta \tag{9}$$

,where t = thickness, and D^e is the stiffness matrix of an element, which either equals to D_f or D_m (see also Section 2.5).

2.3 FE formulation for hygroexpansion

From eqn.8, the term $\{Q^e\}$ = 0 because there are no applied tractions in the model. Since gravity is not considered, the only non-zero external force term is {f ^{e}}, which involves hygro-elastic strains. Hygroexpansion can be defined, depending on the context of discussion, in two ways - the increase in free strain for a given increase in moisture content or for a given relative humidity. Different wood species have different moisture uptakes where moisture uptake also depend on the variation of chemical constituents, namely cellulose, hemicellulose and lignin [21]. Assuming linear elastic stress-strain relation, Hooke's law with hygroexpansion can be written in a matrix format as

$$\sigma = D(\varepsilon - \varepsilon^s) = D\varepsilon - D\varepsilon^s \tag{10}$$

,where ε is given in eqn.(10) and ε^s denotes the hygroelastic which can be determined by either

$$\varepsilon^s = \{\alpha^s\}\Delta w = \begin{bmatrix} \alpha_T \\ \alpha_R \\ 0 \end{bmatrix} \Delta w \tag{11.1}$$

,or $\varepsilon^s = \{\beta^s\}RH = \begin{bmatrix}\beta_T \\ \beta_R \\ 0\end{bmatrix} RH$ (11.2)

,where $\{\alpha^s\}$ is dependent upon the moisture change, Δw whereas β^s depends on the relative humidity, RH.

In this study, the hygroexpansion of the matrix constituent is much less compared to that of wood fibres, so $\beta_m = 0$. Here, hygroexpansion is assumed to be linear and that hygroelastic strains on all direction are independent on one another. The effective global hygroexpansion coefficients are $\beta_x = \beta_{fT}\ and\ \beta_y = \beta_{fR}$. Also, only unidirectional hygroelastic strains are accounted for, $\beta_{TR} = \beta_{xy} = 0$. Recalling global force equilibrium, $P^{int} - P^{ext} = 0$, eqn.(8) can be re-written as

$$[K^e]\{d^e\} = \{f_s^e\} \tag{12}$$

,where in our model $\{f^e\}$ = 0 and $\{f_s^e\}$ arises from the $D\varepsilon^s$ term and the integral form is

$$\begin{aligned}\{f_s^e\} &= \int_{\Omega^e} B^T D_f^e \, dxdy \\ &= \int_{-1}^{1}\int_{-1}^{1} B^T D_f^e \, |\mathrm{J}| \, d\xi d\eta\end{aligned} \tag{13}$$

After $[K^e]$ of all elements are calculated, the global stiffness matrix, $\underline{\mathrm{K}}$ is then assembled, using Fast_Matrix_Assembly MATLAB function with a slight code modification [22]. The global $\underline{\mathrm{F}}$ vector is constructed by assembling non-zero $\{f_s^e\}$ which attributes to those of wood elements only. Boundary conditions shown in Fig.1b) are applied, where x-translation and y-translation are prohibited for the nodes at the left edge and bottom edge of the model respectively. This is implemented by replacing all elements in the associated row of global K matrix, leaving only the only one according diagonal element in the row being equal to 1, such that zero displacements in the $\underline{\mathrm{u}}$ are compulsory.

It should be noted that integration in eqn.(9) and eqn.(13) are performed without the use of Gauss-Legendre quadrature points. Instead, the Symbolic Math Toolbox by MATLAB© is used. This can be explained that as mesh in our model consists of 1x1 square unit entirely, meaning that interpolation functions and Jacobian matrices are all equal for all elements.

The solution of global displacement vector $\underline{\mathrm{u}}$ is then solved linearly with via 'mldivide' function, through

$$\underline{K}\,\underline{u} = \underline{F} \tag{14}$$

,where $\underline{u} = [\, U_x^1\ U_y^1\ U_x^2\ U_y^2\ \cdots\ U_x^N\ U_y^N]^T$, from global nodes 1 to N. The solutions are to be analysed, verified and post-processed.

Experimental measurements of thickness change in [18, 19] after sorption tests are presented. Here, numerical results from the established model are compared with the experimental study to justify a level of agreement.

2.4 Data Post-Processing

Provided with the answers in $\underline{\mathrm{u}}$, the element internal elastic stress, σ^e is calculated by

$$\{\sigma^e\} = \begin{Bmatrix}\sigma_{xx} \\ \sigma_{yy} \\ \tau_{xy}\end{Bmatrix} = [D^e][B^e]\{d^e\} \tag{15}$$

Since a large model with fine elements is dealt with , a single Gauss–Legendre quadrature point (0,0) is used as to simplify post-processing implementation and shorten calculation time. The natural coordinates at (0,0) would be equivalent to the centre of each element in the physical domain. Effectively, B^e in eqn.(15) is the same for all elements as they are identical. Therefore, the only factors determining σ^e are the type of material, hence D^e and the calculated displacements d^e.

The Von-Mises stresses are calculated from the obtained element stresses in eqn.(15), using the following relationship:

$$\boldsymbol{\sigma_{VM}} = \sqrt{\frac{\mathbf{1}}{\mathbf{2}}[\,(\boldsymbol{\sigma_{xx}} - \boldsymbol{\sigma_{yy}})^{\mathbf{2}} + (\boldsymbol{\sigma_{yy}} - \boldsymbol{\sigma_{zz}})^{\mathbf{2}} + (\boldsymbol{\sigma_{xx}} - \boldsymbol{\sigma_{zz}})^{\mathbf{2}}\,] + \mathbf{3}(\boldsymbol{\tau_{xy}^2} + \boldsymbol{\tau_{yz}^2} + \boldsymbol{\tau_{zx}^2})} \tag{16}$$

,with the 2-D plane strain conditions where $\tau_{yz} = \tau_{zx} = 0$,

$$\boldsymbol{\sigma_{VM}} = \sqrt{\frac{\mathbf{1}}{\mathbf{2}}[\,(\boldsymbol{\sigma_{xx}} - \boldsymbol{\sigma_{yy}})^{\mathbf{2}} + (\boldsymbol{\sigma_{yy}} - \boldsymbol{\sigma_{zz}})^{\mathbf{2}} + (\boldsymbol{\sigma_{xx}} - \boldsymbol{\sigma_{zz}})^{\mathbf{2}}\,] + \mathbf{3}\boldsymbol{\tau_{xy}^2}} \tag{17}$$

It should be noted that σ_{zz} is not zero (see eqn.(20-21)). The Von Mises stress given in eqn.(17), however, does not give an insight about the types of local stresses since it is always positive. As a simple approximation, the sign of σ_{VM} depends on the sum of $\sigma_{xx}, \sigma_{yy}, \sigma_{zz}$ [23]. This is to avoid complex calculations of principal stresses that could lead to instability of the simulation. So, signed Von Mises stress, σ_{sVM} can be described below:

$$\sigma_{sVM} = sign(\sigma_{xx}, \sigma_{yy}, \sigma_{zz}) \cdot \sigma_{VM} \tag{18}$$

,where $sign(\sigma_{xx}, \sigma_{yy}, \sigma_{zz})$ can either be equal to +1 or -1. With the above equation, better understandings of stresses can be acquired, reason being that wood fibres are orthotropic which are surrounded by an isotropic polymer matrix. Tension and compression would result in different mechanical behaviours in the microscopic scale.

2.5 Materials properties and considerations

As we assume that the matrix constituent, which is polylactide (PLA) is isotropic, the 2-D plane-strain stiffness is as follows:

$$D_m = \frac{E_m}{(1+v_m)(1-2v_m)}\begin{bmatrix} 1-v_m & v_m & 0 \\ v_m & 1-v_m & 0 \\ 0 & 0 & \frac{1-2v_m}{2} \end{bmatrix} \tag{19}$$

,where E_m, v_m are Young's modulus and Poisson ratio of PLA, which are taken to be 3.6 GPa [18] and 0.35 [24]. On the other hand, Wood is an orthotropic materials. The 3-D compliance matrix, S takes the form,

$$\begin{Bmatrix} \varepsilon_{TT} \\ \varepsilon_{RR} \\ \varepsilon_{LL} \\ \gamma_{TR} \\ \gamma_{TL} \\ \gamma_{RL} \end{Bmatrix} = \begin{bmatrix} \frac{1}{E_T} & -\frac{v_{RT}}{E_R} & -\frac{v_{LT}}{E_L} & 0 & 0 & 0 \\ -\frac{v_{TR}}{E_T} & \frac{1}{E_R} & -\frac{v_{LR}}{E_L} & 0 & 0 & 0 \\ -\frac{v_{TL}}{E_T} & -\frac{v_{RL}}{E_R} & \frac{1}{E_L} & 0 & 0 & 0 \\ 0 & 0 & 0 & \frac{1}{G_{TR}} & 0 & 0 \\ 0 & 0 & 0 & 0 & \frac{1}{G_{TL}} & 0 \\ 0 & 0 & 0 & 0 & 0 & \frac{1}{G_{RL}} \end{bmatrix} \begin{Bmatrix} \sigma_{TT} \\ \sigma_{RR} \\ \sigma_{LL} \\ \tau_{TR} \\ \tau_{TL} \\ \tau_{RL} \end{Bmatrix} = [\,S\,] \begin{Bmatrix} \sigma_{TT} \\ \sigma_{RR} \\ \sigma_{LL} \\ \tau_{TR} \\ \tau_{TL} \\ \tau_{RL} \end{Bmatrix} \tag{20}$$

,where E's are elastic moduli, G's are shear moduli, v's are Poissons ratios. Since compliance matrix is theoretically symmetric, $\frac{v_{RT}}{E_R} = \frac{v_{TR}}{E_T}, \frac{v_{LT}}{E_L} = \frac{v_{TL}}{E_T}, \frac{v_{LR}}{E_L} = \frac{v_{RL}}{E_R}$. For simplification, the global cartesian coordinates X, Y, Z is considered to coincide with the local coordinates of an orthotropic material T, R, L respectively. The compliance matrix, [S] is inverted to yield the stiffness matrix of an orthotropic linear elastic material as:

$$\begin{Bmatrix}\sigma_{TT}\\ \sigma_{RR}\\ \sigma_{LL}\\ \tau_{TR}\\ \tau_{TL}\\ \tau_{RL}\end{Bmatrix}=\begin{bmatrix}C_{11} & C_{12} & C_{13} & 0 & 0 & 0\\ C_{12} & C_{22} & C_{23} & 0 & 0 & 0\\ C_{13} & C_{23} & C_{33} & 0 & 0 & 0\\ 0 & 0 & 0 & C_{44} & 0 & 0\\ 0 & 0 & 0 & 0 & C_{55} & 0\\ 0 & 0 & 0 & 0 & 0 & C_{66}\end{bmatrix}\begin{Bmatrix}\varepsilon_{TT}\\ \varepsilon_{RR}\\ \varepsilon_{LL}\\ \gamma_{TR}\\ \gamma_{TL}\\ \gamma_{RL}\end{Bmatrix}=[\,C\,]\begin{Bmatrix}\varepsilon_{TT}\\ \varepsilon_{RR}\\ \varepsilon_{LL}\\ \gamma_{TR}\\ \gamma_{TL}\\ \gamma_{RL}\end{Bmatrix} \quad (21)$$

As for the 2-D plane strain model in the present study, we have $\varepsilon_{zz} = \gamma_{yz} = \gamma_{zx} = 0$ and hence $\tau_{yz} = \tau_{zx} = 0$, and $\sigma_{zz} = C_{13}\epsilon_{xx} + C_{23}\epsilon_{yy}$. [C] is reduced to a 3x3 matrix in global system as follows:

$$\begin{Bmatrix}\sigma_{xx}\\ \sigma_{yy}\\ \tau_{xy}\end{Bmatrix}=\begin{bmatrix}C_{11} & C_{12} & 0\\ C_{12} & C_{22} & 0\\ 0 & 0 & C_{66}\end{bmatrix}\begin{Bmatrix}\varepsilon_{xx}\\ \varepsilon_{yy}\\ \gamma_{xy}\end{Bmatrix}=\left[\,D_f\right]\begin{Bmatrix}\varepsilon_{xx}\\ \varepsilon_{yy}\\ \gamma_{xy}\end{Bmatrix} \quad (22)$$

,where [D_f] is the element stiffness matrix of wood fibres.
The wood fibres used in the study are bleached birch kraft pulp fibres, whose density is taken to be 1.5 g/cm^3 [25]. The density of PLA is taken to be 1.3 g/cm^3 [18]. Weight fraction of fibres is converted in to volume fraction, V_f for the compatibility of input data via:

$$V_f = \frac{Wt_f/\rho_f}{\frac{1-Wt_f}{\rho_m}+\frac{Wt_f}{\rho_f}} \quad (23)$$

,where Wt_f is the weight fraction, $\rho_f$and ρ_m are the densities of fibre and matrix constituents respectively.

The elastic constants and hygroelastic properties of wood fibres are tabulated in Table 1. Due to lack of experimental data, certain assumptions exist for modelling.

Table 1: Elastic and hygroelastic properties of wood fibres used in this study.

E_{fT}(GPa)	E_{fR}(GPa)	E_{fL}(GPa)	G_{fTR}(GPa)	G_{fTL}(GPa)	G_{fRL}(GPa)	v_{fTR}	v_{fLT}	v_{fLR}	$\beta_{fT}(\varepsilon/RH)$	$\beta_{fR}(\varepsilon/RH)$
3.77	3.77	37.7	0.754	7.54	7.54	0.4	0.3	0.3	0.28	0.28

As wood fibres in our model are assumed to be transversely isotropic, where elastic properties in the R and T directions are taken as equal. Consequently, $E_{fR} = E_{fT}, G_{fTL} = G_{fRL}$. According to the previous study [26], $v_{fTR} = 0.4, v_{fLT} = v_{fLR} = 0.3$. Based on literature, it is also assumed that $G_{fTL}/E_{fT} = 0.2$, and that $E_{fL}/E_{fT} = 10$, which are proper assumptions for general properties of wood.

The hygroexpansion of PLA, β_m in ε/RH is 10^{-4} , which is very small compared to hygroexpansion in the radial and tangential directions of woods [27]. It is, therefore, neglected in our model. The hygroexpansion coefficient of fibre constituent is subjected to a variation of choices based on previous studies [28, 29] . For the model validation discusses below, the selected input of hygroexpansion coefficient, β_{fT}=$\beta_{fR} = 0.28$ [18]. Finally, the outputs of thickness change in % are compared to the out-of-plane hygroexpansion presented in literature.

4. MODEL VERIFICATION AND DISCUSSION

4.1 Comparison of hygroexpansion values

The chosen coefficient of transverse hygroexpansion, $\beta_{fT} = \beta_{fR} = 0.28$, is from the back-calculation method presented in [18], which inputs the thickness swelling from the experiments to the inverse modelling [5] using laminate analogy, which is best applicable for a laminated composite. We, therefore, implement the opposite way round and compare the y-displacement in % of our results to both studies, illustrated in Fig.3.

Firstly, it is seen obviously that, with an increased fibre weight fraction (hereafter shortened as %Wtf), the hygroexpansion increases. This is widely found in many of the previous studies discussed in [27]. Since wood fibres are much more hydrophilic than polymer PLA, such expansion is sensitive to the wood content. Comparing with [18] (see Fig.3a), where the tested specimens were 20mm x 1.5mm rectangular plates, there is only a certain level of agreement with our results – better for the case of 30% fibre weight fraction and worse for the case of 40%Wtf. It is explained in their study that the specimens with 30%Wtf. were better consolidated than all other specimens, resulting in lower moisture ingress to the composites. To rationalize this, better consolidation can lead to better packing density, hence lower porosity. Plus, the interfacial adhesion between fibre and matrix constituents is likely to improve.

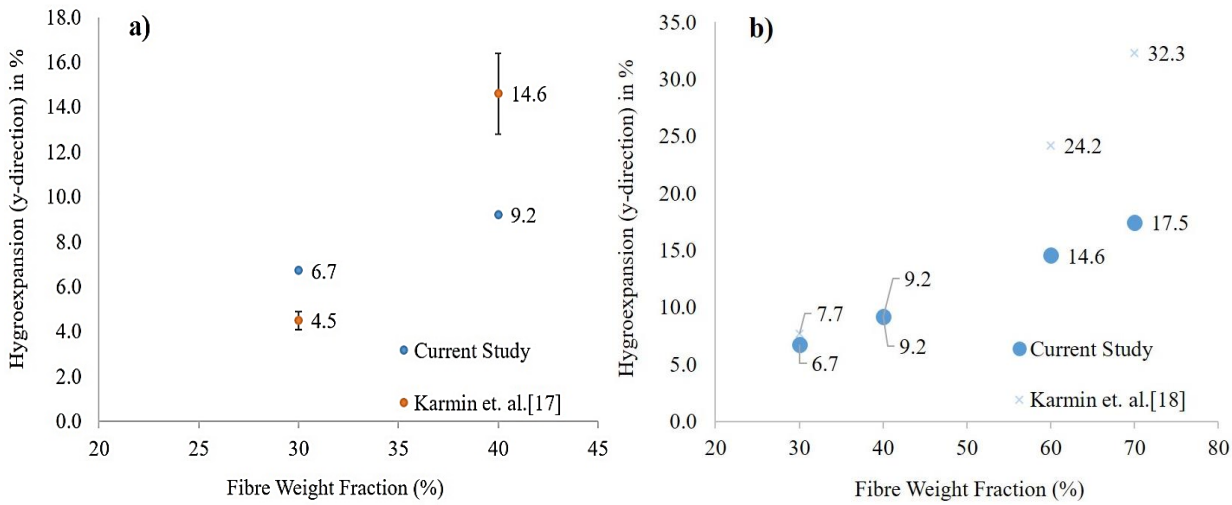

Fig. 3. Hygroexpansion (y-direction) of composites with different % weight fractions by the current model and experimental studies with; a) rectangular plate b) flat circular specimen, at 97%RH. Error bars on experimental results in b) are not provided.

While for the case of 40%Wtf., the modelling results seem to be much different from the experimental results. Some discrepancy should be considered to attribute to the materials input data as well since some values are assumed in order to simplify the model due to lack of experimental data. Nevertheless, the level of data spread indicated by the error bars is seen to be relatively high. And, again, they claim that these samples were more loosely consolidated, verified by micrographs in [18]. It is thought that a relatively high moisture change could transport to the wood fibres, resulting in a higher hygroexpansion. This is also due to the fact that we assume linear hygroelastic behaviours, which neglects the fact that wood hygroexpansion coefficients can vary with factors such as different microfibril angles, moisture contents [9, 26, 27].

For the results shown in Fig.3b), specimens were machined from a composite plate and appeared to be flat and circular [19] .

A good level of agreement can be seen with low %Wtf. At 30% and 40% Wtf., the modelling results agree well with the experimental study, but not so for higher wood contents. This is due to the fact that with relatively large fibre contents, wood fibres exhibit non-linear behaviours. With very high relative humidity, wood fibres will have more moisture uptakes leading to a relatively hygroexpansion [26].

Importantly, the difference in agreement quality amongst the two types of modelled specimen may have arisen by the ways in which the FE models are simplified. As aforementioned, both specimen types are almost identical except the shape and dimensions, this implies a likelihood of the model reliance on the selection of 2-D plane as a cross section for the 3-D experimental specimen. We assume a plane strain model at the cross section because most fibres are thought to align longitudinally with the z-direction (see Fig.1). And since longitudinal hygroexpansion is much less compared to that of other directions, zero strains can effectively be taken as a good assumption.

There is, nonetheless, a thickness difference between the two models, i.e. 4 mm thick for flat circular sample and an average of 1.5 mm thick of the rectangular sample. Since PLA is a type of polymer, and commonly known as a non-porous material, moisture is less likely to ingress all the way through the entire composite structure. Although, the sorption tests were conducted by leaving the specimens in a humid environment for a long period of time, 20 sheet-stacked circular composite specimens may have a lower moisture uptake compared to the rectangular ones with only six sheets stacked up. Though, the z-dimensions of the two shapes are not the same, it should not affect the significant hygroexpansion of radial or tangential directions of wood fibres.

Table 2: Simulation results of birch-PLA composite $40\%Wt_f$, $97\%RH$. Note that $min.\sigma_{VM}$ is actually the maximum compressive Von Mises stress.

Trail	**Change in thickness (%)**	$\boldsymbol{max.\sigma_{VM}}$**(MPa)**	$\boldsymbol{min.\sigma_{VM}}$**(MPa)**	$\boldsymbol{\bar{\sigma}_{VM}}$**(MPa)**
1	9.196	1087	579	450
2	9.199	1078	614	450
3	9.201	1126	658	451
4	9.197	1084	590	450
5	9.200	1142	578	450
6	9.200	1167	610	450
7	9.196	1066	573	450
8	9.197	1114	598	450
9	9.196	1126	597	448
10	9.197	1111	600	450
Average	9.198	1110	600	450
SD.	0.002	32	25	1

Regarding the level of precision, our model exhibits a very low spread of outputs for all simulation trials of both specimen types. Table 2 shows numerical results for the case of 40%Wtf birch-PLA rectangular composite plates. Especially, the standard deviation of change in thickness, which is in fact the hygroexpansion in the y-direction, is very small. While for the stress values; maximum, minimum and mean Von Mises stresses have relatively high SD's. This is because the mesh is well refined so that fibres are well dispersed, having the correct cross section dimension through the entire model. Random trials can lead to a variation of different arrangement of fibres, leading to different maximum stresses. Having said that, there is a high degree of precision presented in the mean Von Mises stress values, i.e. 450(1) MPa for the case of 40%Wtf fibre. Further discussion about stresses are discussed below.

4.2 Stress analysis

Post-processing data reveal that stresses are of overly large magnitudes. Figure 4 (top) shows the entire 20mm by 1.5mm model with the mesh of 666x50 square elements of equal size, while the bottom picture is of the same simulation but with a larger magnification. It can be seen from graph that the Von Mises stresses are high, which are far beyond the yield stress of wood [30] and of PLA [31]. This ensures that during the swelling, composite structure has gone yielding or fracture. Since we assume linear elasticity in the model, it overlooks the fact that the constituent materials may have failed well before they reach the full moisture uptake in the test. Figure 4 shows the microscopic Von Mises stresses of the 40%Wtf composite undergoing 97% RH. The maximum tensile VM stress is about

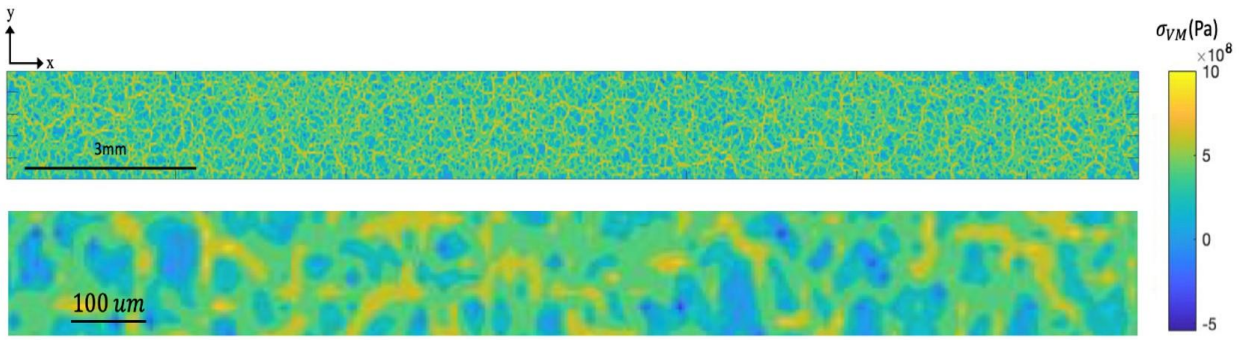

Fig. 4. Local (signed) Von Mises Stress of a 20mm by 1.5 mm model with 40% Wtf , tested at 97%RH; a) entire model, b) magnified partial model

1,000 MPa, while the maximum compressive VM stress is about 500 MPa. Yellow areas indicate the locations of wood fibres which are to expand freely under moisture. As no fracture mechanics or non-linear deformation is considered, the large hygroelastic strains lead to such high stresses. Despite having a very low quantitative accuracy, the values well suggest qualitatively that there is indeed material failure, i.e. yielding of PLA, fracture of wood and interfacial adhesion. This is also supported by the cracks indicated by the micrographs presented in [18]. The numerical results in the current model also show that the majority of material structure undergoes tension much rather compression – 97% of elements have positive VM stresses. This is because the free strains from wood fibres are not much constrained by the matrix constituent as wood fibres have a higher stiffness.

5. CONCLUSIONS

In this work, we have presented a micromechanical model that relies on FE weak formulation accounting for the hygroelastic strains under moisture uptake of wood fibre composite material. A numerical approach is developed using MATLAB code. There exist model simplification and assumptions when the experimental tests are simulated into 2-D plane strain problems. The model reasonably agrees with the experimental studies, having the same tendency of hygroelactic behaviours – increases with an rise in fibre weight fraction. It also seems to agree particularly well when fibre weight fraction is lower than 40% and possibly when the thickness of samples may become a significant factor, which offsets other simplified or neglected factors such as non-linear hygroelastic behaviours and plasticity after material failure, resulting in a slight reduction in hygroexpansion compared to thinner specimens.

In the light of simulation precision, there are very low spread of results. So, a high level of confidence is ensured, in spite of a high level of fibre dispersity and random arrangement. Von Mises stresses are calculated and they confirm that the hygroexpansion cause the structural failure of the constituents, almost entirely by tension. However, the magnitudes of stresses should be taken into quantitative considerations with care where necessary because they are well beyond the critical values of most materials. Therefore, with more relevant considerations involving materials behaviours and properties of both constituents at a low moisture uptake, this model can be a reliable tool to predict hygroexpansion quantitatively and possibility of material failure qualitatively. Further studies are likely contribute to investigating debonding and cracking behaviours under wet-dry cycles.

REFERENCES

[1] Bledzki, A., Sperber, V. and Faruk, O. Natural and wood fibre reinforcement in polymers, Rapra Review Reports, 2002.
[2] Rodrigues, C.S. and Pereira, M.A. The role of moisture and temperature variations in the accelerated weathering cycles for durability studies of cellulose-cement composites, paper presented in International Conference on Durability of Building Materials and Components 2011, Porto, Portugal.
[3] Cooke, A. Durability of autoclaved cellulose fiber cement composites, paper presented in 7th Inorganic-Bonded Wood and Fiber Conference, 2000.
[4] Mohr, B., Nanko, H. and Kurtis, K.E. Durability of kraft pulp fiber–cement composites to wet/dry cycling, Cement & Concrete Composites, Vol. 27(4), 2005, pp. 435-448.
[5] Klyosov, A. Wood-Plastic Composites, 2007, John Wiley & Sons, New York.

[6] Morrell, J.J., Nicoel, M.S., David, E.P. and Armando, G.M. Durability of wood-plastic composites, Wood Design Focus, Vol. 16, 2006, pp. 7-10.
[7] Laboratory-Forest-Product. Wood Handbook: Wood as an Engineering Material, 2010, United States Department of Agriculture Forest Service, Wisconsin.
[8] Nicole, S. Influence of moisture absorption on mechanical properties of wood flour-polypropylene composites, Journal of Thermoplastic Composite Materials, Vol. 14, 2001, pp. 421-432.
[9] Lindner, M. Factors affecting the hygroexpansion of paper, Journal of Materials Science, Vol. 53(1), 2018, pp. 1-26.
[10] Baldwin, J.D., Altan, C. and Rajamani, C.A. Structural analysis of an injection molded short-fiber-reinforced disk, Journal of Materials Processing and Manufacturing Science, Vol. 6(2), 1997, pp. 123-145.
[11] Dasgupta, A., Agarwal, R.K. and Bhandarkar, S.M. Three-dimensional modeling of woven-fabric composites for effective thermo-mechanical and thermal properties, Composites Science and Technology, Vol. 56(3), 1996, pp. 209-223.
[12] Stahl, D.C. and Cramer, S.M. A three-dimensional network model for a low density fibrous composite, J. Eng. Mater. Technol, Vol. 120(2), 1998, pp. 126-130.
[13] Termonia, Y. Structure-property relationships in short-fiber-reinforced composites, Journal of Polymer Science Part B: Polymer Physics, Vol. 32(6), 1994, pp. 969-979.
[14] Xiaoshuang, X., Shirley, Z., Lin, H., Jefferson, Z., Xiang, L., Xiaojin, W. and Menghe M. Finite element models of natural fibers and their composites: A review, Journal of Reinforced Plastics and Composites, Vol. 37(9), 2018. pp. 617-635.
[15] Stålne, K. and Gustafsson, P.J. Three-dimensional model for analysis of stiffness and hygroexpansion properties of fiber composite materials, Journal of Engineering Mechanics, Vol. 128(6), 2002, pp. 654-662.
[16] Srubar, W.V. and Billington, S.L. A micromechanical model for moisture-induced deterioration in fully biorenewable wood–plastic composites, Composites Part A: Applied Science and Manufacturing, Vol. 50, 2013, pp. 81-92.
[17] Erik, T.J., Wernersson, L.G., Miettinen, A., Cris, L., Hendriks, L. and Gamstedt, E.K. Swelling of cellulose fibres in composite materials: Constraint effects of the surrounding matrix, Composites Science and Technology, Vol. 74, 2013, pp. 52-59.
[18] Almgren, K.M., Gamstedt, E.K. and Varna, J. Contribution of wood fiber hygroexpansion to moisture induced thickness swelling of composite plates, Polymer Composites, Vol. 31(5), 2010, pp. 762-771.
[19] Almgren, K.M., Gamstedt, E.K., Berthold, F. and Lindstro M. Moisture uptake and hygroexpansion of wood fiber composite materials with polylactide and polypropylene matrix materials, Polymer Composites, Vol. 30(12), 2009, pp. 1809-1816.
[20] Karmin, M. Wood-fibre composites: Stress transfer and hygroexpansion, 2010, KTH Fibre and Polymer Technology, Stockholm.
[21] Cousins, W.J. Elastic modulus of lignin as related to moisture content, Wood Science and Technology, Vol. 10(1), 1976, pp. 9-17.
[22] Al-Rumaithi, A. Fast Global Stiffness Matrix Assembly, MathWorks, MATLAB Central, URL: https://www.mathworks.com/matlabcentral/fileexchange/70447-fast-global-stiffness-matrix-assembly, accessed on 13/4/2019
[23] Boresi, A.P., Schmidt, R.J. and Sidebottom, O.M. Advanced mechanics of materials, 5th edition, 1993, John Wiley & Sons, New York.
[24] Fung, Y.C. Foundations of Solid Mechanics, 1965, Prentice-hall, New Jersey.
[25] Kellogg, R.M. and Wangaard, F.F. Variation in the cell-wall density of wood, Wood and Fiber Science, Vol. 1969(3), 1969, pp. 180-204.
[26] Gamstedt, E.K. Modelling of effects of ultrastructural morphology on the hygroelastic properties of wood fibres, Journal of Materials Science, Vol. 42(24), 2007, pp 10254-10274.
[27] Skaar, C. Wood-Water Relations, 1988, Springer, Berlin.
[28] Persson, K. Micromechanical modelling of wood and fibre properties, 2000, Lund University, Sweden.
[29] Yew, G., Mohd, A., Yusof, Z., Ishak, M. and Ishiaku, U. Water absorption and enzymatic degradation of poly(lactic acid)/rice starch composites, Polymer Degradation and Stability, Vol. 90(3), 2005, pp. 488-500.
[30] Green, D.W., Winandy, J.E. and Kretschmann, D.E. Mechanical Properties of Wood, General technical report FPL, USDA Forest Service, 1999.
[31] Ugural, A.C. and Fenster, S.K. Advanced Mechanics of Materials and Applied Elasticity, 5th Edition, 2012, Pearson Education, London.